WHAT'S NEEDED IN THE UV AND EUV

by

G.A. Doschek
E.O. Hulburt Center for Space Research
Naval Research Laboratory

ABSTRACT

High spectral and spatial resolution UV and EUV spectroscopy is discussed with emphasis on the spectroscopic observations that are required in order to increase our understanding of the physics of the lower transition region. The properties of the lower transition region are reviewed, and the available lower transition region plasma diagnostics are reviewed for the wavelength range between about 1150 and 2000 Å. One important conclusion is that comprehensive spectroscopic coverage over a rather broad temperature range is necessary in order to observe satisfactorily small transition region structures. This is illustrated by two examples from the recent NRL Spacelab 2 HRTS experiment.

I. INTRODUCTION

The hotter layers of the Sun's atmosphere, the transition region and corona, can only be satisfactorily studied in the UV, EUV, and X-ray spectral regions. The lower transition region may be defined as the atmospheric region at temperatures roughly between 10^4 and 10^5 K. The upper transition region contains plasma between about 10^5 and 10^6 K. Regions between about 10^6 K and 3×10^6 K are defined as the solar corona. Plasma hotter than 3×10^6 K is associated with transient energetic events such as surges, eruptive prominences, and of course flares. In this paper I will emphasize what can be learned about the hotter regions of the Sun's atmosphere from high resolution spectroscopy and imaging in the UV and EUV. Although not impossible in principle, it is highly unlikely that an X-ray telescope and/or X-ray spectrometer will accompany the HRSO on its first flight.

I will emphasize in particular what can be learned about the transition region, and possibly the corona, since these are areas of particular interest to me. However, regarding the chromosphere I would like to point out that in addition to the well-known diagnostic lines of Mg II near 2800 Å, the UV and EUV contain very rich and complete emission line spectra of C I, S I, Fe II, Si I and Si II, as well as important continuum emission. Very little work on the diagnostic potential of these spectra has been done so far, and the analysis of these spectra is a promising research topic.

The question posed as the title of this paper, "What's Needed in the UV and EUV", can only be answered by considering the known properties of the atmospheric regions we wish to study, and by reflecting on our ideas concerning the physics of these regions. In addition, instrumental limitations and atomic spectroscopy play an important role in answering this question. In the first High Resolution Solar Physics Workshop, Athay (1985) outlined some of the properties and physics of the chromosphere and transition region. In this paper I will also undertake such a

review, but with emphasis on how the atmospheric characteristics and physics affect the UV and EUV spectrum.

Before proceeding further, however, I will give a somewhat utopian answer to the question of what's needed in the UV and EUV. If funding, flight opportunities, and instrumental limitations did not present the severe problems that they do, it would be desirable to obtain high resolution spectra, with spectral resolution of about 1/3 the Doppler width of chromospheric and transition region lines, between about 400 and 4000 Å, with accompanying high spatial resolution images, about 0.1", in selected spectral lines formed between 10^4 and 10^6 K. Of course all this is also desired with high time resolution, on the order of a few seconds. As will be seen below, it is not realistic to obtain this type of information for the first flight of HRSO. However, a great deal can be accomplished even with considerably "descoped" instrumentation.

II. INSTRUMENTAL AND SPECTROSCOPIC LIMITATIONS

The region from about 1150 to 4000 Å can be well-observed using optics coated with aluminum and a protective coating of MgF_2. The normal incidence reflectivity of aluminum at these wavelengths is about 80% or better. Below about 1150 Å, however, the reflectivity of aluminum decreases rapidly and it becomes necessary to use other coatings in order to achieve normal incidence reflectances of not more than about 20%. It is possible to achieve much higher reflectances than 20% by using grazing incidence optics, but then spatial imaging becomes a severe problem. Multilayer optics is a promising technology for some solar spectroscopic applications, but the current spectral resolution is very bad for wavelengths greater than 400 Å ($\Delta\lambda/\lambda \approx 0.07$). Because of the properties of aluminum mentioned above, there are few high spectral resolution UV solar observations at wavelengths much shorter than 1150 Å. The IUE wavelength cutoff is around 1150 Å for the same reason. In addition, for astronomical spectrometers the hydrogen continuum edge at 912 Å can cause severe absorption for wavelengths less than 912 Å in even relatively nearby sources, depending on the direction of the source in the sky. This continuum absorption is also important in the solar atmosphere (e.g., Schmahl and Orrall 1979, Doschek and Feldman 1982).

Because of the above limitations, there is an instrumental dividing line at around 1150 Å. If one wishes to observe both below and above this wavelength, more than one instrument is needed, and the instruments will be significantly different in design. This fact has important consequences for the study of the transition region and corona, when atomic spectroscopy is considered.

The lower transition region can be observed through spectral lines of ions such as C II, C III, C IV, O III, O IV, O V, N III, N IV, N V, Si III, Si IV, S III, and S IV. Many of the resonance and/or allowed (by pure electric dipole spontaneous decay) lines of these ions fall at wavelengths less than 1150 Å. However, diagnostically important intersystem lines fall at longer wavelengths. As examples, allowed lines of O III fall near 526, 703, and 835 Å, and strong intersystem lines fall at 1660 and 1666 Å. Allowed lines of O IV fall near 554 and 790 Å and strong intersystem lines fall near 1402 Å. It is of course desirable to observe both the allowed and intersystem lines simultaneously, because of the temperature sensitivity of line ratios and the information the ratios provide concerning the Lyman continuum absorption, but it is also impractical with a single instrument.

By considering the spectroscopy in detail, we reach the conclusion that only one strong line formed at temperatures above about 2×10^5 K can be observed at wavelengths longer than 1150 Å. This is the Fe XXI line at 1354 Å and it can only

be observed during flares. However, there are a number of weak coronal and upper transition region lines from ions such as Si VIII, Fe IX - Fe XII that appear at longer wavelengths, but a very sensitive instrument with large dynamic range is required to observe these lines against the solar disk. For example, the Fe XII line at 1242.0 Å is only 1/80 the strength of the neighboring N V line at 1242.8 Å at 4" above the white light limb (Doschek et al. 1976). Lists of these forbidden coronal lines are given by Feldman and Doschek (1977) and Sandlin, Brueckner, and Tousey (1977).

Although only a handful of intersystem lines of transition region ions fall at wavelengths longer than 1150 Å, their diagnostic potential is enormous for deducing properties of the transition region. I shall devote most of the following discussion to the 1150 - 2000 Å region, with emphasis on the lower transition region.

III. THE TRANSITION REGION AND UV - EUV OBSERVATIONS

a) Physical Structure

The physical structure of the transition region is presently unknown. About ten years ago the transition region was viewed solely as an interface between chromospheric and coronal plasma. The chromospheric and coronal plasma was assumed to be confined by some type of magnetic structure, such as a closed flux tube, spicule, or field lines compressed over supergranule cell boundaries, such as in the Gabriel (1976) model. There is no way that the coronal and chromospheric plasma can be in contact without generating plasma at intermediate temperatures. In models without flow, where classical thermal conduction is the dominant energy transport mechanism, the transition region is very thin in height, of the order of 100 km. It turns out that the transition region is also very thin in models that encorporate flow, e.g., Mariska (1984). In fact it seems perfectly reasonable to believe that hot coronal loops, such as observed by X-ray telescopes, interface with the chromosphere and contain this type of transition region. This is so because the physical characteristics of such loops appear to obey scaling laws based on physics that produce such transition regions (Rosner, Tucker, and Vaiana 1978).

However, there are observations indicating that the actual situation is far more complicated (e.g., Feldman 1983). Perhaps the most outstanding observations are images of extended structures in transition region lines such as C IV and Ne VII, and the fact that none of the classical transition region models, with or without flow, can produce the observed chromospheric-transition-region emission measure distribution (Athay 1982). It appears that cool transition region structures may exist that are separated by magnetic fields from at least the coronal plasma. Since heat conduction across magnetic fields is very small, it is no longer obvious that plasma at transition region temperatures must occur in very thin layers, although the structures containing transition region plasma are undoubtedly quite small. Thus the observed transition region emission is composed of two types of emission: emission from "classical" transition regions and emission from structures with properties that are largely unknown. A central problem to be answered from HRSO UV instrumentation is the nature of these unknown structures. Thus the HRSO UV instrumentation should be able to obtain high spatial resolution transition region images that can be located with respect to chromospheric and photospheric features.

There are three current theories regarding what these structures might be, proposed by Antiochos and Noci (1986), Rabin and Moore (1984), and Athay (1984).

I will not discuss the details of these models here, but only emphasize that the models provide, or can be developed to provide, predictions regarding the physical properties of the transition region. For example, in the model of Antiochos and Noci (1986) the transition region structures are cool loops. This model predicts that the pressure in a loop varies inversely as a high power of the maximum loop temperature. In the model of Moore and Rabin (1984) the pressure is the same for all temperatures. In the model of Athay (1984) the pressure is time dependent, but on average, should increase with temperature. In order to determine the validity of these and other models it is clearly desirable to derive densities as a function of temperature from UV and EUV observations.

The sizes of transition region structures are known to be very small. Direct imagery from HRTS (by building up spectroheliograms) shows structures with sizes down to the HRTS spatial resolution (0.8" for HRTS 1). From a flare observed from Skylab, Doschek, Feldman, and Rosenberg (1977) concluded that a surge observed at lower transition region temperatures during flare onset had a characteristic length of about 60 km, or < 0.1". This result was based on obtaining a density N_e from intersystem lines and a volume emission measure $N_e^2 V$ from allowed lines. Most density-emission measure analyses indicate very small filling factors for transition region plasma, 0.1 - 0.001. Thus UV, EUV instrumentation should have as high a spatial resolution as possible, at least 0.5".

The location of transition region structures is well-known. From limb observations, peak emission from lower transition region structures occurs at 2" - 4" above the white light limb. However, emission extends to heights of at least 10" in the quiet Sun and extends to 20" or more in coronal holes. Figure 1 shows the source functions obtained from Abel inversions of limb brightening curves obtained from Skylab data (see Feldman, Doschek, and Mariska 1979). The full width at half maximum FWHW of the functions in Figure 1 is about 5". As an example of the small filling factor of transition region plasma, if this region were uniformly filled with plasma, the path length L through this plasma above the limb would be $L = \sqrt{2RH}$, where R is the solar radius and H is the 5" layer thickness, and L equals about 7×10^4 km. The actual path length may be obtained from the ratios of doublet lines from Al III, Si IV, C IV, and N V, obtained from Skylab spectra, as described by Doschek, Mariska, and Feldman (1981). Figure 2 shows that above the limb the peak intensities of these lines depart from the optically thin ratio, 2:1. From these observations path lengths can be derived and these are given in Table 1. The path lengths for Al III, Si IV, and N V indicate filling factors of 6%; for C IV the filling factor is 1.1%. The difference between the C IV and other path lengths is probably significant. C IV is formed at about 10^5 K, where the differential emission measure is at its smallest value.

b) Plasma Diagnostics

The discussion so far indicates the importance of density and temperature, or pressure measurements. There are several excellent density diagnostics for the lower transition region, based on the intersystem lines that arise from metastable levels. These levels can be depopulated by collisions as well as radiative decay when densities are high, which provides a density diagnostic. The densities above which several prominent transition region lines become affected by collisional depopulation are shown in Figure 3. Plotted is the ratio of the population of the metastable level to the product of the electron density and the density of the ion in which the line arises, as a function of electron density. For a line unaffected by collisional depopulation and/or formed at very low densities this

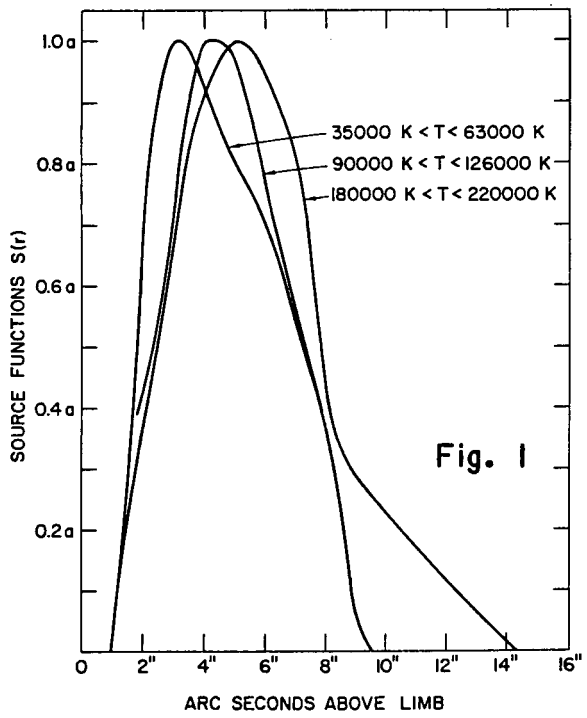

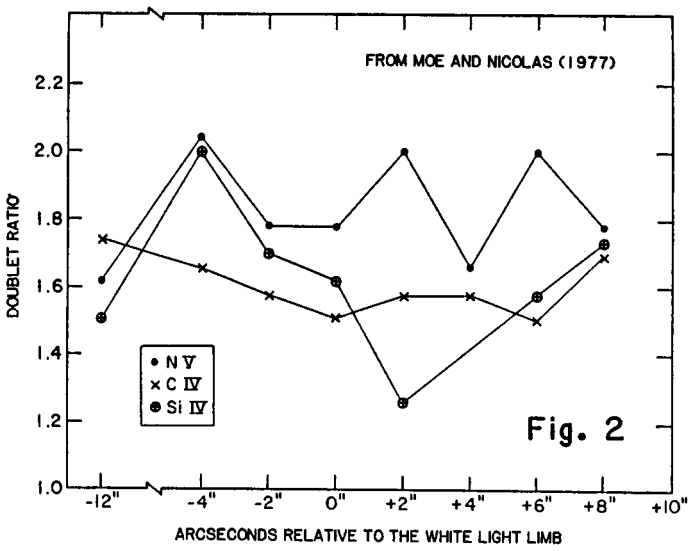

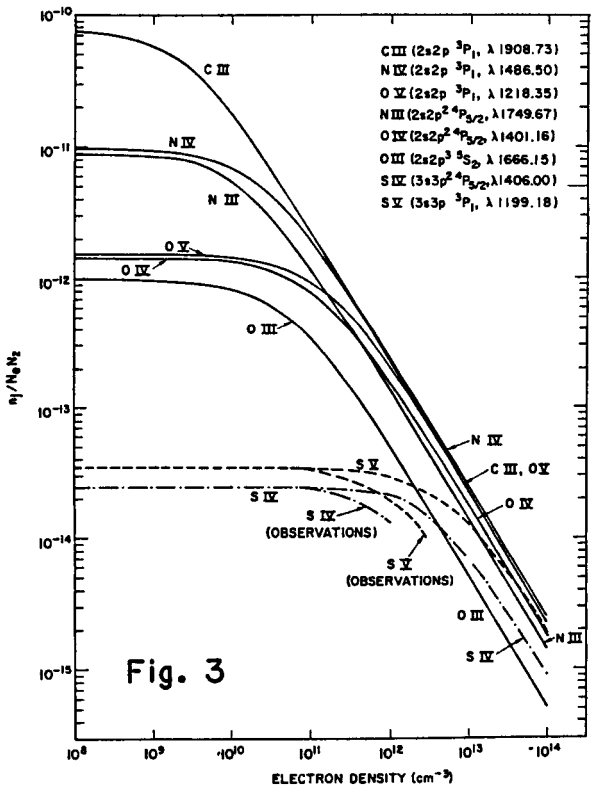

Fig. 1 - The distribution of lower transition region plasma with height above the limb (Feldman, Doschek, and Mariska 1979).

Fig. 2 - Intensity ratio of indicated doublets above the limb. The optically thin ratio is 2:1 (Doschek, Mariska, and Feldman 1981).

Fig. 3 - Populations of levels and ions indicated as a function of electron density (Doschek 1985).

TABLE 1

Opacity and Path Lengths at $2''$ - $4''$ Above the Limb

T_e (K)	L(km)[a]
4×10^4	3,500
7×10^4	4,500
10^5	800
1.8×10^5	4,800

[a] The path lengths can be uncertain by factors of about 2.

TABLE 2

Electron Pressures

Region	$\log(N_e T_e)$
Quiet Sun (Chromosphere)	15.2
Quiet Sun (Transition Region)	15.1
Quiet Sun (Corona)	15.0 ($h > 20''$)
Coronal Hole (Transition Region)	15.1 (14.8)
Active Region (Chromosphere)	15.2
Active Region (Transition Region)	15.9
Active Region (Corona)	15.2 - 16.0
Prominence (Transition Region)	14.9
Sunspot (Transition Region)	15.0
Surges (Flare-related Activity) (Transition Region)	15.0 - 16.2
Flares (Transition Region)	16.0 - 18.0
Flares (Corona, 10^6 K < T_e < 6×10^6 K)	16.8 - 18.7

ratio is a horizontal line as a function of density. However, when the density is high enough to produce collisional depopulation, the ratio begins to fall and eventually falls linearly on a logarithmic scale. In this region the ratio of the intersystem lines to allowed lines unaffected by density and formed at the same temperature is a very sensitive function of density. The good news is that many lines are available for density diagnostics; the bad news is that most lines are not sensitive for densities below 10^{10} cm^{-3}. The canonical quiet Sun transition region pressure is 10^{15} cm^{-3} K, so for O IV at 1.3×10^5 K the average density is about 8×10^9 cm^{-3}, where the O IV lines are not sensitive. Only C III provides a line that is fairly sensitive in the important regime between 10^9 and 10^{10} cm^{-3}. However, this line is rather weak against the solar disk and must be observed over a strong continuum background. The situation is much improved for active regions and explosive events, where typical pressures are around 10^{16} cm^{-3} K. In this case many of the lines in Figure 3 provide good diagnostics.

There are two types of density sensitive line ratio available. One involves the ratio of two intersystem lines. Examples occur for N III, O IV, Si III, and S IV lines between 1150 and 2000 Å. A typical result for O IV lines is shown in Figure 4, and the O IV lines from Skylab spectra for three different solar regions are shown in Figure 5. The left most panel in Figure 5 shows the quiet Sun limb spectrum. The 1407 Å/1405 Å ratio is in the low density limit. The other two spectra are from energetic events and indicate densities of about 5×10^{10} cm^{-3}. The problem with these ratios is that they become insensitive at very high densities or at very low densities. However, the O IV ratio in Figure 4 may be sufficiently sensitive to work in the $10^9 - 10^{10}$ cm^{-3} region, if measurements are good and the atomic data are as good as claimed. A partial test of the atomic data can be found by observing the O IV lines in stellar spectra of stars with atmospheres of very low density. The ratios should then be in the low density limit predicted by theory. High resolution IUE spectra are perfectly adequate for such a test. The O IV line ratios in the star RR Tel (Penston et al. 1983) are very close to the low density limits computed by Nussbaumer and Storey (1982). This example demonstrates the interplay between solar and stellar spectra in the area of plasma diagnostics, a topic often overlooked in discussions of the solar-stellar connection.

The other type of density diagnostic is the ratio of an intersystem line to an allowed line of a different ion, but an ion formed at the same temperature as the intersystem line ion. There are several pitfalls to this technique, but it is very useful for high density structures ($10^{11} - 10^{13}$ cm^{-3}, see Figure 3). Because the differential emission measure can vary in different solar regions, it is necessary that the intersystem and allowed line are formed at the same temperature, or if not that the emission measure at the temperature of the intersystem line can be interpolated from the emission measures of allowed lines. This can be accomplished by constructing plots such as shown in Figure 6. In Figure 6 line intensities are plotted normalized to the C IV intensity in the quiet Sun. Crosses mark allowed lines and solid dots refer to intersystem lines. If the differential emission measure (DEM) of the region in question has the same shape as the quiet Sun DEM, then the crosses should define a horizontal line in the plot, as is the case for the particular active region chosen. However, for the active region the intersystem line intensities fall substantially below the intensities predicted for allowed lines, because the active region densities are higher than the quiet Sun densities. The vertical lines connecting the intersystem line dots to the horizontal line segments define the decrements that can be used to directly infer electron densities using Figure 3. Note that the shape of the surge DEM departs from the quiet Sun shape, but that electron

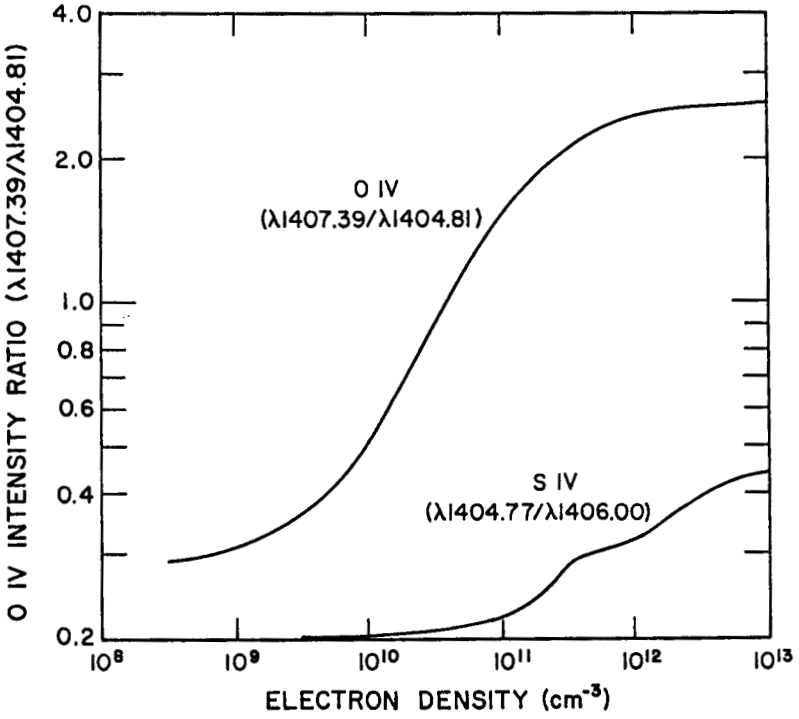

Fig. 4 - A density sensitive O IV line ratio. The S IV line ratio can be used to correct the λ1405 line for blending. See Doschek (1984) for sources of atomic data.

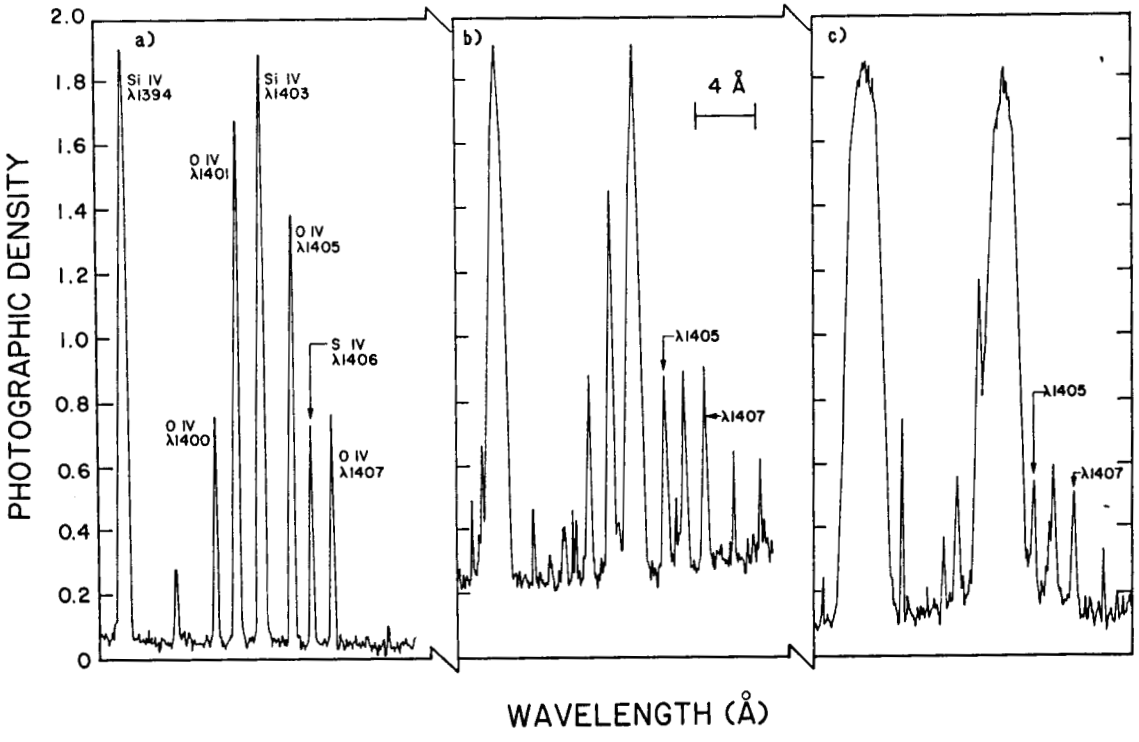

Fig. 5 - The O IV multiplet from Skylab S082-B spectra (Doschek 1984).

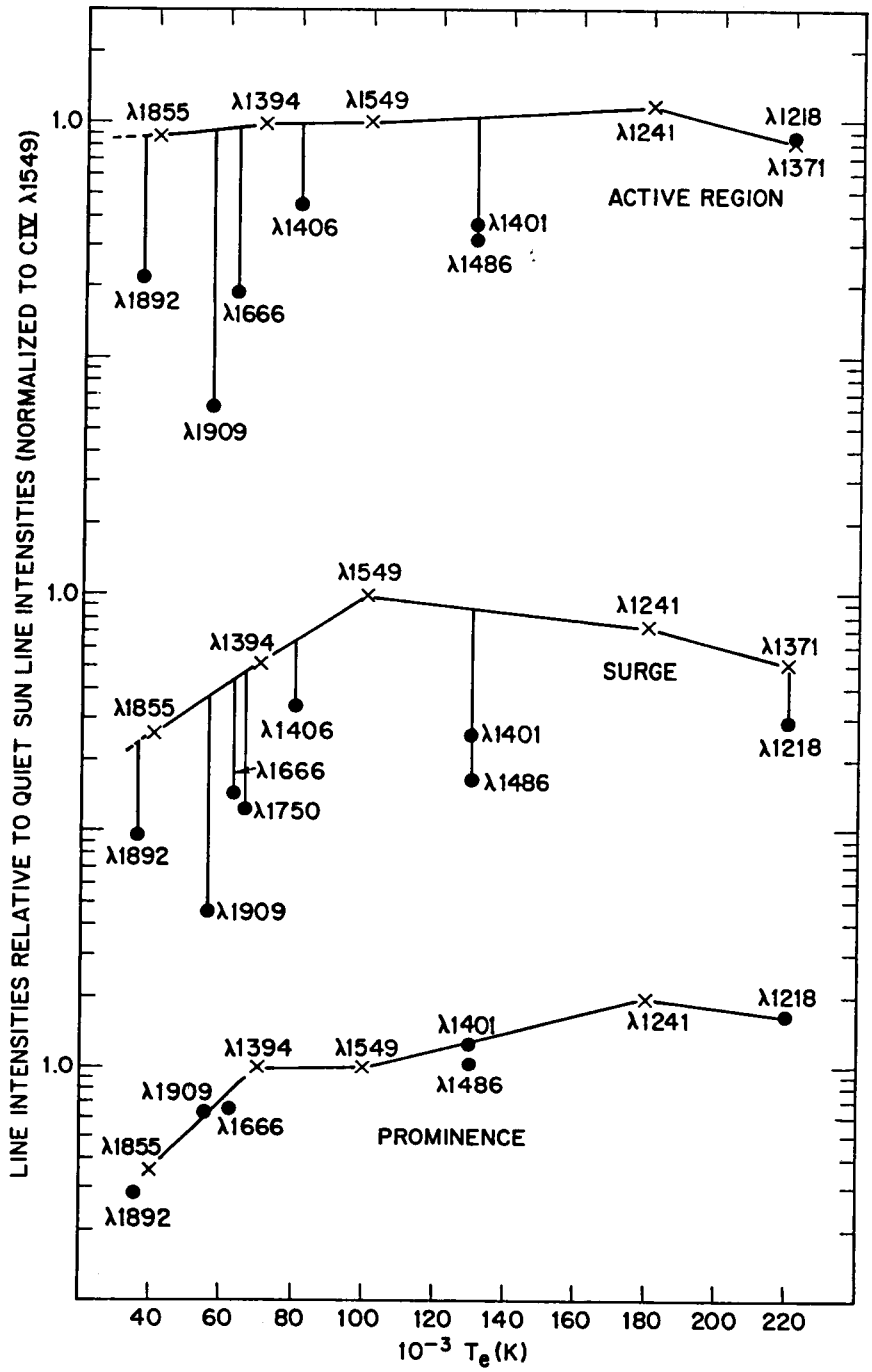

Fig. 6 - Skylab solar spectra of an active region, surge, and prominence compared to the quiet Sun spectrum (Doschek 1985).

densities are still high. The shape of the prominence DEM also departs from the quiet Sun shape, but the densities are the same as in the quiet Sun. A summary of electron pressures in different solar regions is given in Table 2.

Figure 6 shows that the shape of the DEM in different regions can depart from quiet Sun values. Inspection of the HRTS data indicates that on the scale of fine structures there is no "canonical" DEM distribution, although if many different structures in a region are averaged together, the shape of the DEM appears in many cases to be similar to the quiet Sun DEM over limited temperature ranges.

Examples of how different the shape of the DEM can be in different regions are found in the HRTS Spacelab 2 data. Figure 7 shows what Brueckner and Bartoe (1983) define as a turbulent event, i.e., an event exhibiting large, nearly symmetrically broadened line profiles. The event is well-observed in lines of low temperature ions such as C II, Si III, and Si IV, but is weaker in C IV lines, much weaker in O IV lines, and not seen at all in lines of N V. This implies that the DEM begins to decrease rapidly above 7×10^4 K, the temperature at which Si IV is formed. If only the O IV and Si IV lines were observed, and the small O IV/Si IV ratio were interpreted as due to a high density, then a spuriously high density would be obtained. The problem is that the O IV lines are formed at a temperature almost twice as high as the temperature at which Si IV is formed. Nevertheless, a density can be inferred for this event, by using density sensitive line ratios of Si III that are analogous to the O IV lines in their density sensitivity. The density is about 10^{11} cm^{-3} at the temperature of formation of Si III, about 3×10^4 K.

Another interesting example of how unpredictable the shape of the DEM can be in energetic events is shown in Figure 8. The event in question is a strong downflowing region as evidenced by the predominant redshifted structures in the line profiles. Note that this event can be easily seen in high temperature lines, such as N V formed at about 1.8×10^5 K, but is completely absent in lines of lower temperature ions such as C II and Si III. The O IV line ratios can be used to obtain densities at a temperature of about 1.3×10^5 K.

The above examples illustrate the unpredictability of the shape of the DEM when fine structures are resolved or partially resolved. The conclusion is that UV instrumentation should be able to observe a large number of lines, that, if possible, do not leave gaps in temperature. That is, for the region above 1150 Å, lines from cold ions ranging from S I and Si I up through N V should be observed. The Si I and S I lines are not only good chromospheric diagnostics, but the very narrow lines allow quite accurate wavelength measurements that in turn enable velocities relative to the chromosphere to be measured with an accuracy that can be as high as 1-2 km s^{-1} (Dere, Bartoe, and Brueckner 1986).

b) Transition Region Dynamics

Up to now the discussion has centered on the sizes, densities, and the DEM of transition region structures. However, one of the most outstanding characteristics of the transition region is its highly dynamic character. Random or turbulent, as well as anisotropic flows, are a common characteristic of at least the lower transition region. The motions can be divided into two distinct classes: those associated with apparently typical quiescent regions, and those associated with transient events. The motions associated with transient events are subdivided into the so-called "turbulent" events or into the category of "jets" (Dere, Bartoe, and Brueckner 1983, 1984, 1986). The "jets" appear in emission lines of chromospheric (C I) and transition region (C IV) ions.

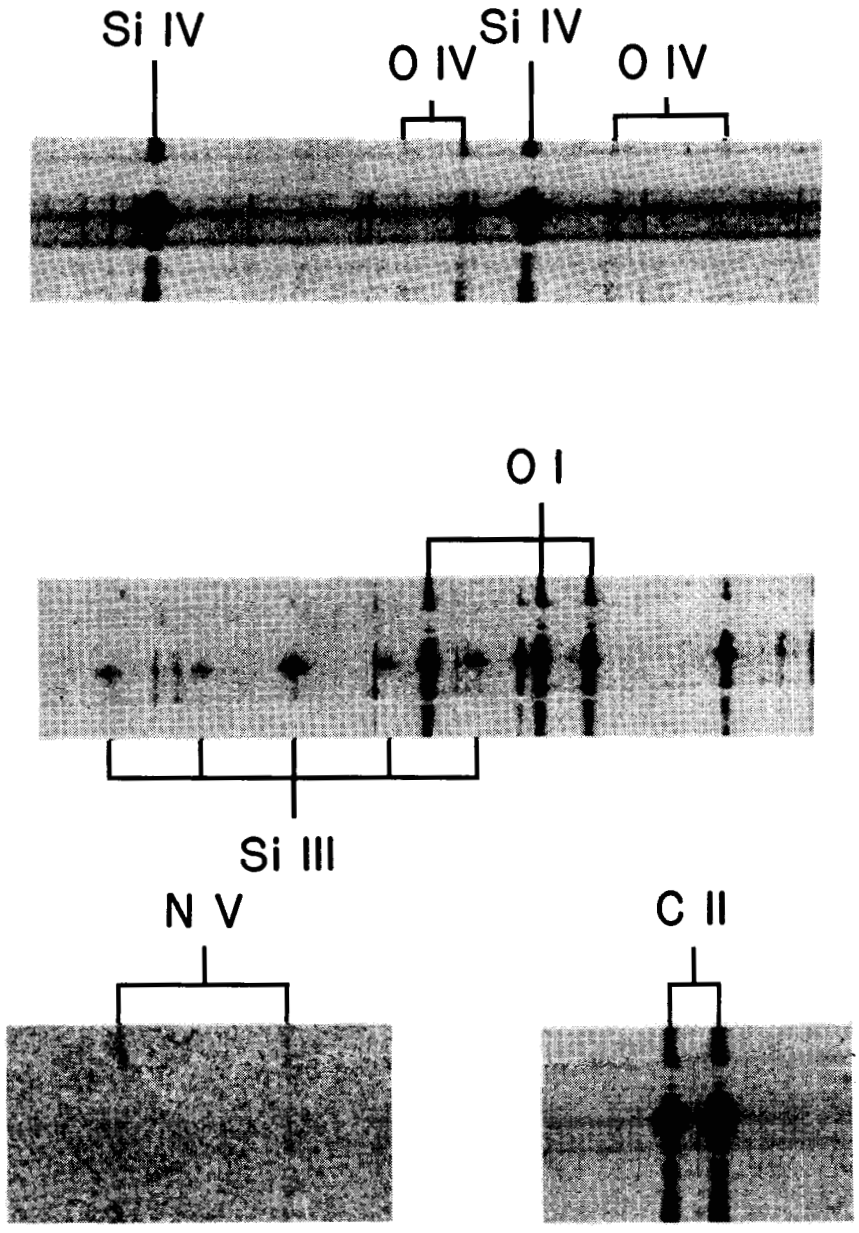

Fig. 7 - A "turbulent" transition region event recorded by the HRTS Spacelab 2 instrument. The event is seen at temperatures characteristic of C II($\approx 2 \times 10^4$K), Si III($\approx 2\text{-}4 \times 10^4$K), and Si IV($7 \times 10^4$K). It is not seen at temperatures characteristic of O IV(1.3×10^5K) and N V(1.8×10^5K). Approximate wavelengths are: C II(1335 A), Si III (1300 A), Si IV(1400 A), O IV(1400 A), N V(1240 A).

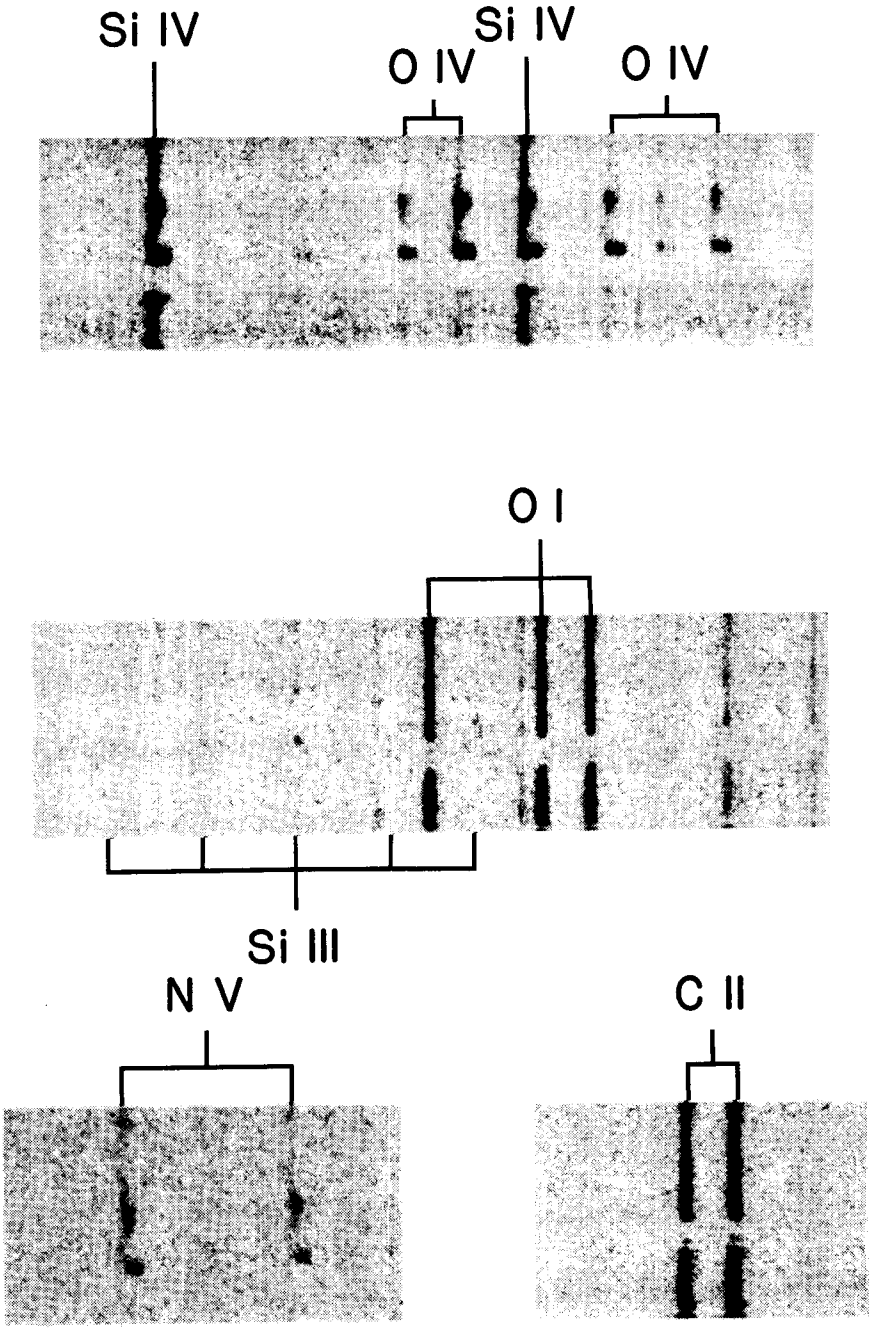

Fig. 8 - An event exhibiting large downflows recorded by the HRTS Spacelab 2 instrument. The event is seen in higher temperature lines such as Si IV, O IV, and N V, but is not seen in lower temperature lines of C II and Si III.

Turbulent events appear as both blue- and redshifted emission with velocites of about 100 km s^{-1}. Note that the transient events we are discussing are not flares, surges, or sprays. They are relatively new phenomena discovered with the HRTS. Of course larger events such as flares and surges also appear in transition region lines, but we confine our attention here to events not obviously associated with solar flares.

The motions associated with quiescent regions are also of two types. There is a random mass motion or perhaps turbulence associated with chromospheric and transition region lines. Lower transition region line widths are dominated by this motion, and not by their intrinsic Doppler widths. The average motions (averaged over many fine structures) range from about 8 km s^{-1} for upper chromospheric temperatures up to about 25 km s^{-1} at temperatures of 2 x 10^5 K. The increase in average motion appears to be monotonic with temperature (Figure 9), but there is considerable scatter in the results, principally because when viewed on a fine scale, such as with HRTS, the motions vary considerably from one individual structure to another. Nevertheless, the average values, as obtained from Skylab, OSO-8, SMM, and HRTS data are well-represented by the data in Figure 9.

Most of the lower transition region line width measurements have been obtained from the intersystem and allowed lines we have been discussing. An enlarged and more detailed portion of Figure 9 is shown in Figure 10. The data in Figure 10 are obtained from Skylab and are discussed in Doschek, Mariska, and Feldman (1981). The values shown by the circles enclosing dots are from data obtained above the limb. Above the limb the allowed lines are broadened by opacity, as discussed previously.

Above 3.5 x 10^5 K there is a gap in our knowledge concerning the motions up to about 8 x 10^5 K. Above this temperature, we again have measurements. These data come from the weak forbidden coronal lines at wavelengths greater than 1150 Å mentioned in Section II. The gap arises because of the difficulty of observing below 1150 Å with both high spectral resolution and high sensitivity.

Inspection of Figure 9 indicates that the motions peak around log $T_e \simeq 5.4$, but this is uncertain because of the gap. We also know that the motions at any given temperature appear to increase with height above the limb. Finally, the mass motions either disappear or are very small in quiescent prominences. They are also less in sunspot spectra and can be narrow at times during flares.

The origin of these motions is unclear and represents one of the outstanding problems in the UV to be addressed by HRSO UV instrumentation. They may arise because different unresolved fine structures have nonzero motions relative to each other, or they may be truly turbulent in nature. Recent HRTS Spacelab 2 results (Brueckner et al. 1986) indicate that both line broadening mechanisms may be present.

The other pervasive and interesting quiescent motion is the tendency for most lower transition region lines to be redshifted relative to chromospheric lines from ions such as Si I and S I (Doschek, Feldman, and Bohlin 1976). The redshift generally indicates motions of about 6-10 km s^{-1} and SMM observations have shown that these motions can persist for long time intervals over certain regions. The redshifts can also vary considerably from point to point on the Sun. Detailed studies of these redshifts, commonly interpreted as due to a net downflow of material, have been carried out with the SMM data (e.g., Gebbie et al. 1981, Klimchuk 1986). The velocity patterns appear to be organized over large regions of the solar surface (Athay 1985). One point to keep in mind concerning the redshifts is that they are smaller than the random motions on the average. That is, the net Doppler shift of the line centroid is less than the line width. The

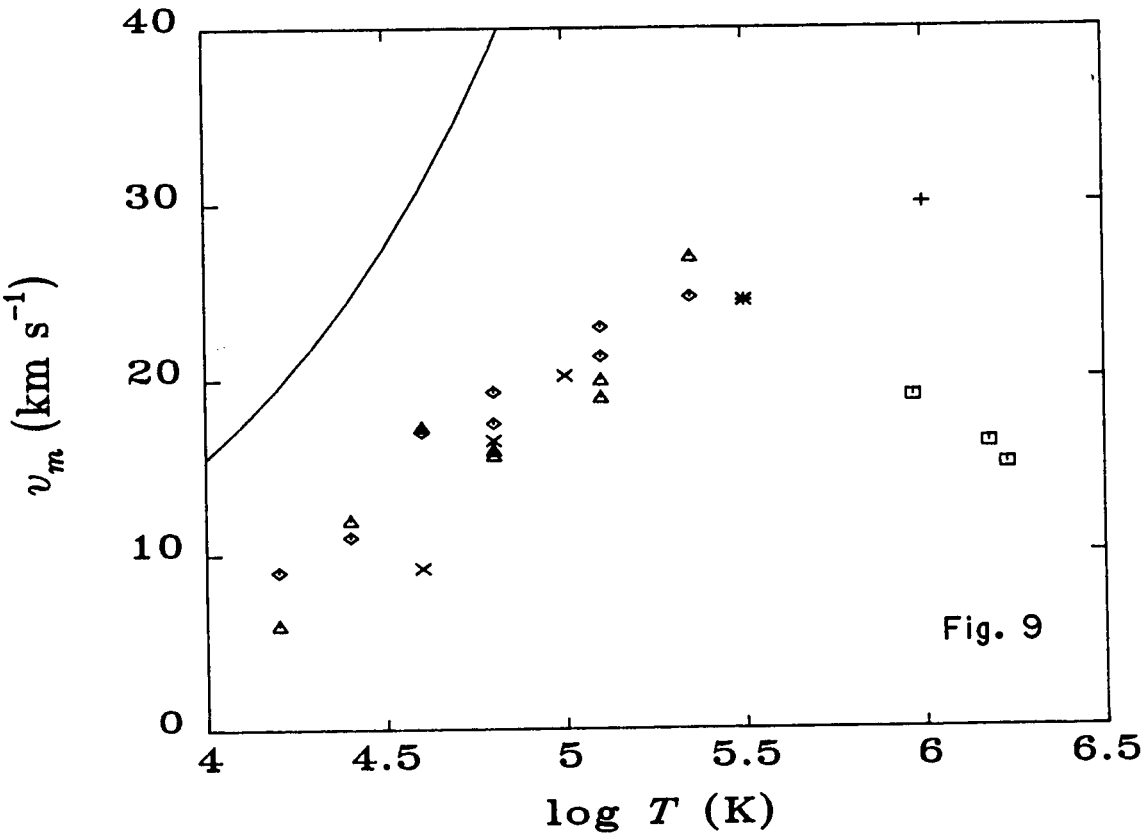

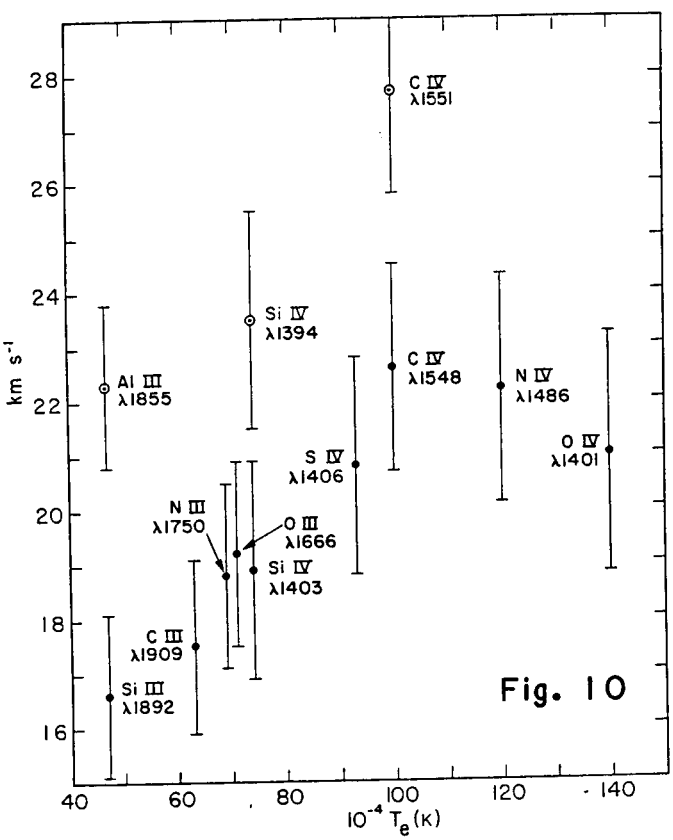

Fig. 9 - Nonthermal broadening as a function of temperature. The solid line is the sound speed. See Mariska (1986) for details.

Fig. 10 - A detailed view of nonthermal motions in the lower transition region. The error bars are due to measurement statistics and real variations from region to region. Open circles are for lines measured above the limb and broadened by opacity.

implication is that there are unresolved structures, exhibiting both upflows and downflows, but that either more plasma is moving downward, or the plasma moving downward has a larger emission measure than the upward flowing plasma. A second strange point about the redshifts is that they do not appear to vanish at the limb (Feldman, Cohen, and Doschek 1982). The reason for this is unclear. And a third interesting point is that the redshifts are also seen in the spectra of other stars (e.g., Ayres et al. 1983). Whatever the cause of the redshifts, it is clear that these motions are closely linked with the origin and structure of the lower transition region, and it is important to study the dynamics of the transition region at a spatial resolution of about 0.1". Therefore, UV instrumentation should have sufficient spectral resolution to adequately measure chromospheric and lower transition region line profiles. A resolution of 0.03 Å between 1150 and 2000 Å would be adequate.

d) Some Non-equilibrium Effects

The turbulent events and their short lifetimes indicate that the plasma associated with these events may not be in ionization equilibrium. If the plasma is not in ionization equilibrium, then interpretation of the UV emission lines is complicated since ionization fractions and temperatures of ion formation can no longer be taken as known quantities. Several workers have considered possible scenarios in which ionization equilibrium might not be valid. Mariska (1984) considered the case of a flux tube in which a steady flow is established by asymmetric heating. He examined the effect of this flow on UV and XUV lines of O III, O IV, O V, and O VI. In his cases, the transition region is "classical", i.e., a thin layer separating the chromosphere from a hotter, nearly coronal plasma. Mariska (1984) found departures of about a factor of 4 or so between emission measures derived under the assumption of ionization equilibrium and the actual emission measures. However, the departures in the upflowing portion of the loop differed in sign from those in the downflowing leg, and if the results are averaged, as would occur with a low spatial resolution instrument, no substantial disagreement in emission measure was obtained. Similarly, for the ions he chose, temperature sensitive line ratios did not yield temperatures much different than expected assuming ionization equilibrium.

Dere et al. (1981) have also considered transient transition region plasmas. They adopted a non-"classical" transition region model in which hot coronal plasma cools rapidly to chromospheric temperatures and conduction is unimportant. An interesting result of their calculation is that pulses of emission are generated in UV emission lines at times differing by a few tens of seconds (Figure 11). Broad spectral line coverage, along with time resolution of a few seconds, would be able to detect such cooling plasma and would provide an unambiguous signature of transient ionization in the plasma. Therefore, UV instrumentation should have time resolution no worse than about 20s.

Another non-equilibrium process that might affect UV line intensities is the existence of non-Maxwellian electron velocity distributions. Such distributions might be maintained in a quasi-stationary state because of steep temperature gradients that produce appreciable temperature variations over the mean free path of an electron (e.g., Schoub 1983). Such non-Maxwellian distributions can alter the ionization balance and the excitation rates of spectral lines. In particular, precipitations of such particles into relatively cool regions (about 3-4 x 10^4 K) can affect high excitation emission lines from ions such as Si III by a factor of 2 or so (Dufton, Kingston, and Keenan 1984). Dufton, Kingston, and Keenan (1984) were able to explain the intensity of a high excitation Si III line by invoking a

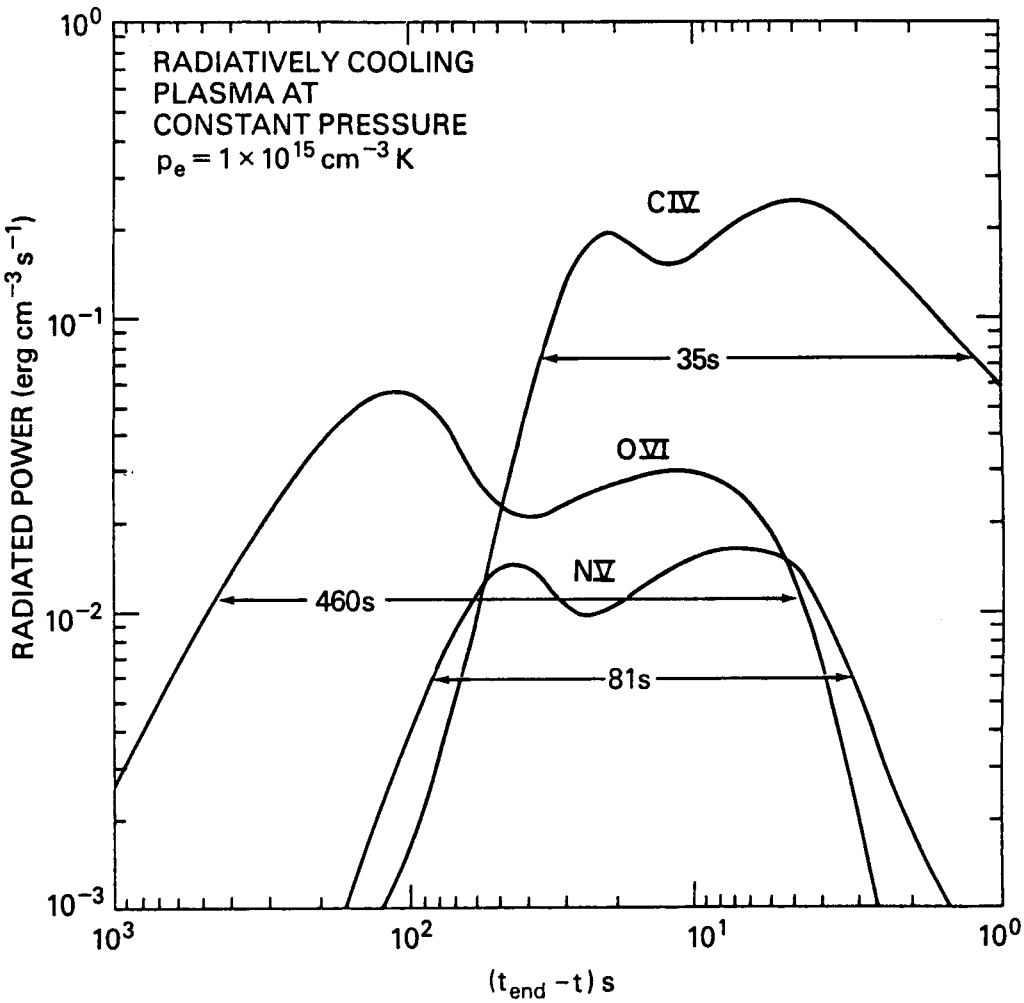

Fig. 11 - Time histories of emission from lithiumlike ions from a radiatively cooling plasma. The elapsed time t_{end} corresponds to $T_e = 10^4$K (Dere et al. 1981).

non-Maxwellian distribution, but Doschek and Feldman (1986) did not find such an effect for a similar line of Al III. It is desirable to measure temperatures, if possible, for transition region ions, in order to investigate such effects. Transport of ions into higher temperature regions, such as discussed by Jordan (1975) for He II, would similarly enhance high excitation lines. Unfortunately, the high excitation lines that appear longward of 1150 Å are weak, and the resonance lines fall shortward of the 1150 Å cutoff. The Si IV 3d --> 3p lines, which are really excited from the 3s $^2S_{1/2}$ ground state, fall near 1128 Å. Other candidates for temperature measurement are the same transitions in Mg II and Al III, and the line of Si III mentioned above. Another possible candidate, mentioned in Doschek and Feldman (1986), is a ratio involving S III lines. However, all of the high excitation lines are weak and therefore a sensitive spectrograph is required. It would be interesting to see if such weak lines might be detected by the Space Telescope in certain stellar objects that have strong UV emission line spectra such as RR Tel.

A final point should be made concerning UV spectra. Frequently the most interesting lines are the intercombination lines. For these lines resonances in the excitation cross sections and precise values of radiative decay rates are very important. It is therefore necessary for the support of HRSO to maintain strong support for theoretical atomic physics calculations of highly ionized atoms, and also to support laboratory measurements of radiative decay rates and excitation processes for such ions.

I thank Guenter Brueckner and the NRL Spacelab 2 team for providing access to the HRTS Spacelab 2 data. I thank Spiro Antiochos, Kenneth Dere, and Uri Feldman for useful comments on the manuscript.

REFERENCES

Antiochos, S.K., and Noci, G. 1986 Ap. J., 301, 440.
Athay, R.G. 1982, Ap. J., 263, 982.
Athay, R.G. 1984, Ap. J., 287, 412.
Athay, R.G. 1985, in Proceedings of the MPA/LPARL Workshop on Theoretical Problems in High Resolution Solar Physics, 16-18 September 1985, page 205.
Ayres, T.R., Stencel, R.E., Linsky, J.L., Simon, T., Jordan, C., Brown, A., and Engvold, O. 1983, Ap. J., 274, 801.
Brueckner, G.E., and Bartoe, J.-D.F. 1983, Ap. J., 272, 329.
Brueckner, G.E., Bartoe, J.-D.F., Cook, J.W., Dere, K.P., and Socker, D.G. 1986, COSPAR Topical Meeting on Solar Investigations from Spacelab 2, July 1986, to appear in Advances in Space Research.
Dere, K.P., Bartoe, J.-D.F., and Brueckner, G.E. 1983, Ap. J. (Letters), 267, L65.
Dere, K.P., Bartoe, J.-D.F., and Brueckner, G.E. 1984, Ap. J., 281, 870.
Dere, K.P., Bartoe, J.-D.F., and Brueckner, G.E. 1986, Ap. J., 305, 947.
Dere, K.P., Bartoe, J.-D.F., Brueckner, G.E., Dykton, M.D., and Van Hoosier, M.E. 1981, Ap. J., 249, 333.
Doschek, G.A. 1984, Ap. J., 279, 446.
Doschek, G.A. 1985, in Autoionization, edited by A. Temkin (Plenum Press Corp., New York), Chapter 6.
Doschek, G.A., and Feldman, U. 1982, Ap. J., 254, 371.
Doschek, G.A., and Feldman, U. 1986, Ap. J. (Letters), to be submitted.
Doschek, G.A., Feldman, U., and Bohlin, J.D. 1976, Ap. J. (Letters), 205, L177.
Doschek, G.A., Feldman, U., and Rosenberg, F.D. 1977, Ap. J., 215, 329.
Doschek, G.A., Feldman, U., Van Hoosier, M.E., and Bartoe, J.-D.F. 1976, Ap. J.

Suppl., 31, 417.
Doschek, G.A., Mariska, J.T., and Feldman, U. 1981, M.N.R.A.S., 195, 107.
Dufton, P.L., Kingston, A.E., and Keenan, F.P. 1984, Ap. J. (Letters), 280, L35.
Feldman, U. 1983, Ap. J., 275, 367.
Feldman, U., Cohen, L., and Doschek, G.A. 1982, Ap. J., 255, 325.
Feldman, U., and Doschek, G.A. 1977, J. Opt. Soc. Am., 67, 726.
Feldman, U., Doschek, G.A., and Mariska, J.T. 1979, Ap. J., 229, 369.
Gabriel, A.H. 1976, Phil. Trans. Roy. Soc. of London A, 281, 339.
Gebbie, K.B. et al. 1981, Ap. J. (Letters), 251, L115.
Jordan, C. 1975, M.N.R.A.S., 170, 429.
Kjeldseth Moe, O., and Nicolas, K.R. 1977, Ap. J., 211, 579.
Klimchuk, J.A. 1986, Ph.D. Thesis, University of Colorado and National Center for Atmospheric Research, NCAR/CT-96.
Mariska, J.T. 1984, Ap. J., 281, 435.
Mariska, J.T. 1986, Ann. Rev. Astron. Astrophys., 24, 23.
Nussbaumer, H., and Storey, P.J. 1982, Astr. Ap., 115, 205.
Penston, M.V., et al. 1983, M.N.R.A.S., 202, 833.
Rabin, D., and Moore, R. 1984, Ap. J., 285, 359.
Rosner, R., Tucker, W.H., and Vaiana, G.S. 1978, Ap. J., 220, 643.
Sandlin, G.D., Brueckner, G.E., and Tousey, R. 1977, Ap. J., 214, 898.
Schmahl, E.J., and Orrall, F.Q. 1979, Ap. J. (Letters), 231, L41.
Schoub, E.C. 1983, Ap. J., 266, 339.